Device

Article

Passive thermal management of electronic devices using sorption-based evaporative cooling

Graphical abstract

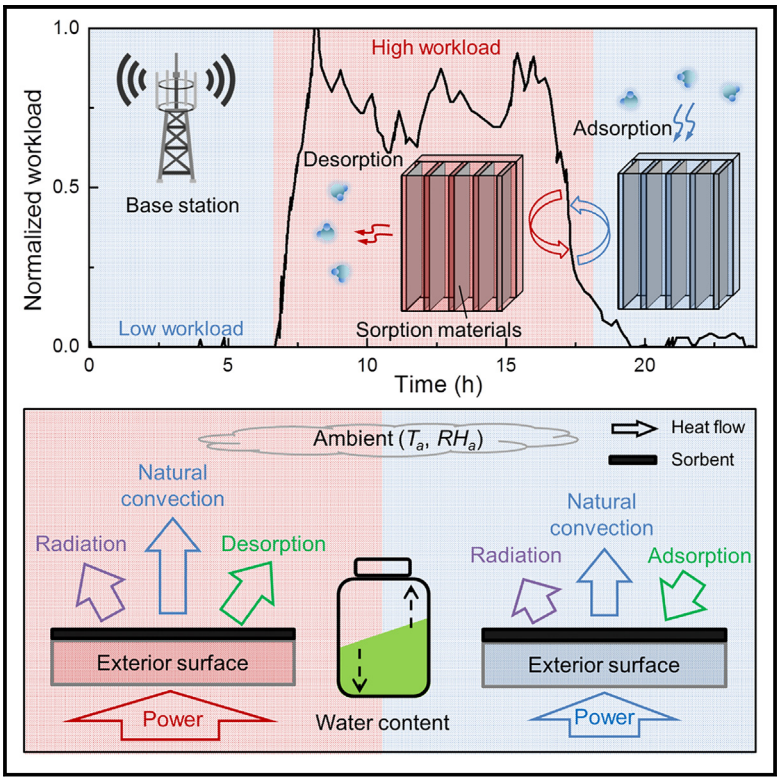

Highlights

- Cooling performance is evaluated both experimentally and numerically
- The proposed method could achieve a maximum 20°C temperature reduction
- The cooling power of the proposed method could reach up to 602 W/m^2
- The proposed method is evaluated in a state-of-the-art 5G base station

Authors

Haoran Liu, Jiaqi Yu, Chenxi Wang, Ziya Zeng, Primož Poredoš, Ruzhu Wang

Correspondence

rzwang@sjtu.edu.cn

In brief

In addition to ambient temperatures, passive cooling can also be accomplished using moisture. Herein, the application of a salt-embedded composite sorbent to an electronic device results in the desorption process—moisture transferred from the sorbent to the air—occurring during the device's high-workload period and thus increasing the heat dissipation capacity. The sorbent can then later recover through adsorption during the low-workload period. Our results demonstrate that this method could achieve significant cooling on 5G base stations.

Explore
Early prototypes with exciting performance and new methodology

Liu et al., 2023, Device *1*, 100122
December 22, 2023 Published by Elsevier Inc.
https://doi.org/10.1016/j.device.2023.100122

CellPress

Please cite this article in press as: Liu et al., Passive thermal management of electronic devices using sorption-based evaporative cooling, Device (2023), https://doi.org/10.1016/j.device.2023.100122

Device

CellPress
OPEN ACCESS

Article

Passive thermal management of electronic devices using sorption-based evaporative cooling

Haoran Liu,[1,2] Jiaqi Yu,[1,2] Chenxi Wang,[1] Ziya Zeng,[1] Primož Poredoš,[1] and Ruzhu Wang[1,3,*]
[1]Institute of Refrigeration and Cryogenics, Shanghai Jiao Tong University, 800 Dongchuan Road, Shanghai 200240, China
[2]These authors contributed equally
[3]Lead contact
*Correspondence: rzwang@sjtu.edu.cn
https://doi.org/10.1016/j.device.2023.100122

THE BIGGER PICTURE Cooling is essential for electronic devices nowadays. To meet the temperature constraints, the number of simultaneously operated chips (or cores) is usually limited, which seriously influences system performance and results in the famous "dark silicon" problem. To enlarge the heat dissipation capacity, this work demonstrates a passive and sustainable method that uses ambient moisture for cooling state-of-the-art 5G base stations. The results demonstrate that, compared with the original devices, the proposed method could bring about a maximum of 20°C temperature reduction and 602 W/m^2 cooling power. The utilization of ambient moisture could bring new opportunities for passive cooling and break the potential limitation caused by the original temperature-difference-driven heat transfer process.

SUMMARY

Thermal management is becoming the main bottleneck of electronic devices, especially in situations where only passive strategies are available, such as base stations and smartphones. In this article, we develop passive, sorption-based evaporative cooling based on a salt-embedded composite sorbent and further apply the method to a state-of-the-art 5G base station. Both the experimental and simulation results demonstrate that the proof of concept on a finned heat sink could achieve an exceptional equivalent cooling power of 602 W/m^2, which accounts for about 22% of the total heat dissipation capacity and could bring a maximum of 20°C temperature reduction compared with the original device. An additional experiment on a well-developed practical base station demonstrates that the proposed cooling strategy could still bring about a 5°C–8°C temperature reduction. Sorption-based evaporative cooling could greatly expand the potential of passive cooling capacity and create new opportunities for future electronics.

INTRODUCTION

Due to the ever-increasing power density of batteries and components in modern electronics, thermal management is becoming a major bottleneck that restricts the performance of electronic devices.[1–3] During operation, the computing abilities of semiconductors might be wasted due to the device's cooling capacity being too limited to keep up with its own heat efflux, and thus the so-called "dark silicon" problem occurs.[4] Limited by reliability, energy consumption, size, and cost, some electronic devices, such as base stations and smartphones, could only be cooled by passive strategies, such as natural convection and heat radiation.[5] Additionally, considering the tremendous energy and water consumption of cooling electronic devices,[6] improving passive cooling capacity will yield significant positive impacts on both the environment and the system performance.

Improving the cooling capacity of passive strategies is a non-trivial task. For natural convection, the heat transfer coefficient could be improved by optimizing the structure of heat sinks.[7–9] However, after prolonged research, the heat sink of state-of-the-art electronic devices has been carefully designed and is difficult to further optimize. For heat radiation, the recently emerged sky radiative cooling technique brings inspiring results,[10,11] while its relatively low cooling capacity, i.e., about 40–120 W/m^2, still hinders its extensive applications in cooling electronic devices. Fortunately, besides the ambient temperature, the abundant moisture contained in the atmosphere could also serve as a cooling source.[12] Mimicking the sweating of mammals, sorption-based evaporative cooling could passively provide a large cooling capacity based on the high enthalpy of moisture desorption.[13] Then, the spontaneous adsorption enables the recovery process and thus achieves sustainable operation. Based on the aforementioned principle, sorption-based evaporative cooling has been evaluated on many devices and systems such as space cooling,[14–19] photovoltaic (PV) panels,[20–26] thermoelectric generators (TEGs),[27–29] wearable

Please cite this article in press as: Liu et al., Passive thermal management of electronic devices using sorption-based evaporative cooling, Device (2023), https://doi.org/10.1016/j.device.2023.100122

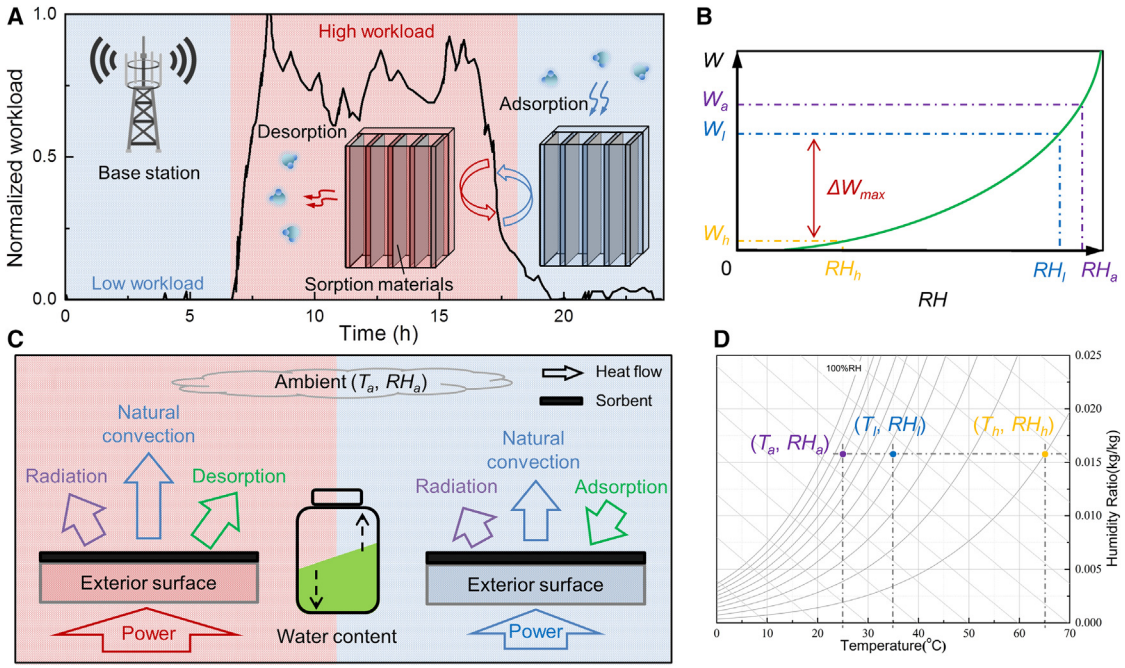

Figure 1. Schematic diagram of applying sorption-based evaporative cooling on base stations

(A) Typical normalized workload of a base station in business district[54] and the working principle.

(B) Schematic water sorption isotherms.

(C) Heat transfer enhancement and thermal storage effect.

(D) Determination of the steady-state RH of sorbent based on the psychrometric chart.

electronics,[30] smartphones,[5,31,32] practical or simulated chips,[21,33–36] and batteries.[37–43] Among them, generally considered sorption materials include solid-state porous sorbents such as metal-organic frameworks (MOFs)[34,44] and polymeric-based sorbents such as hygroscopic polymer gels (HPGs).[45–47] For MOFs and their modified forms, although fast sorption/desorption kinetics are preferred, the high cost, complexity of synthesis, and weak adhesion with other surfaces might influence their large-scale application. For HPGs, high water uptakes and flexibility make them promising materials for cutting-edge energy-water-related technologies, while the potential risks of swelling and durability still present serious challenges.

Besides the aforementioned MOFs and HPGs, salt-embedded composites, which confine hygroscopic salts such as lithium chloride (LiCl) and calcium chloride ($CaCl_2$) into the porous matrix, are also popular sorbent materials.[48] Their unique advantages, such as stability, ease of synthesis, and relatively high adsorption capacity especially at low relative humidity (RH), make the salt-embedded composites become competitive materials in many energy-water devices and systems such as atmospheric water harvesting,[49–51] thermal storage,[52] and dehumidification.[53] In this article, the performance of sorption-based evaporative cooling on a state-of-the-art base station is evaluated based on a popular salt-embedded composite, i.e., LiCl with the matrix of active carbon fiber (ACF) felt. Specifically, based on the workload fluctuation characteristic of the base station, the proposed sorption-based evaporative cooling could increase the heat dissipation capacity at peak hours and recover at resting time. A small-scale proof-of-concept experiment is first conducted. The results demonstrate that a maximum equivalent average cooling power of 602 W/m^2 could be achieved, which is higher than that of the previous studies and will result in a maximum of 20°C temperature reduction compared with the original device. The proposed cooling strategy is further applied on a state-of-the-art commercial base station. The results show that a 5°C–8°C temperature reduction could be achieved even if the original heat sink is carefully designed. The utilization of the proposed sorption-based evaporative cooling could break the heat dissipation limitation caused by natural convection and radiation and thus create new opportunities for the future development of electronic devices.

RESULTS

Working principle

Due to the fluctuation of user demand, the power consumption of base stations has a stable peak in a day; power consumption during the remaining time is relatively low.[33,54] That is, the continuous operation of the device will not result in the requirement of continuous cooling. The corresponding fluctuation of temperatures then provides opportunities for sustainable usage of sorption-based evaporative cooling, i.e., cyclic desorption and adsorption (recovery). The basic working principle of applying sorption-based evaporative cooling on state-of-the-art base stations is demonstrated in Figure 1. Specifically, the sorption materials (sorbent) are attached or coated on the exterior surface of

Please cite this article in press as: Liu et al., Passive thermal management of electronic devices using sorption-based evaporative cooling, Device (2023), https://doi.org/10.1016/j.device.2023.100122

the heat sink. Under a certain operating temperature, the final steady-state RH of the sorbent could be determined by a psychrometric chart as shown in Figure 1D. Then, the equilibrium point could be determined by the water sorption isotherms as shown in Figure 1B. When the workload and the corresponding temperature are relatively high, the equilibrium point of the sorbent (denoted as (RH_h, W_h)) will migrate to a lower RH level, while the equilibrium point of the sorbent will stay at a relatively high RH level (denoted as (RH_l, W_l)) under low workloads. In the best condition, where the workload of the base station is zero, the equilibrium point of the sorbent will achieve its maximum, which is the same as the ambient RH (denoted as (RH_a, W_a)).

During the operation of sorption-based evaporative cooling, when the current water content of the sorbent (W_i, $g_{water}/g_{sorbent}$) is higher than its equilibrium point, the endothermic desorption process will occur and thus enhance the heat dissipation of the whole device, as shown in Figure 1C. In this situation, the cooling capacity (q_c, W) at exterior surfaces could be expressed as

$$q_c(t) = Ah(t)(T_s(t) - T_a(t)) + A\sigma\varepsilon\left(T_s(t)^4 - T_a(t)^4\right) + \dot{m}(t)H_{de}, \quad \text{(Equation 1)}$$

where A, h, T_s, T_a, ε, σ, t, $\dot{m}$, and H_{de} denote the surface area (m^2), heat transfer coefficient of natural convection ($W\cdot m^{-2}\cdot K^{-1}$), surface temperature (K), ambient temperature (K), emittance, Stefan-Boltzmann constant ($W\cdot m^{-2}\cdot K^{-4}$), time (s), desorption rate of the sorbent (g/s), and desorption enthalpy per gram of desorbed water (J/g_{water}), respectively. From the perspective of heat transfer, the cooling capacity of sorption-based evaporative cooling is intrinsically increased by involving the mass transfer, and thus the obstacles caused by natural convection and radiation could be overcome. The desorption rate could be further calculated by

$$\dot{m} = m_s\frac{dW_i}{dt} = K_yA(Y_s - Y_a), \quad \text{(Equation 2)}$$

where m_s, K_y, Y_s, and Y_a denote the mass of sorbent (g), mass transfer coefficient ($g\cdot m^{-2}\cdot s^{-1}$), humidity ratio of air contained in sorbent surface pores, and ambient air ($g\cdot kg^{-1}$). A more detailed heat transfer analysis and design criteria of the proposed cooling strategy are demonstrated in Note S1.

On the other hand, in situations where W_i is lower than the equilibrium point, the adsorption processes will occur and thus achieve the recovery of the sorbent. The adsorption heat released at the surfaces of sorbents will be dissipated through natural convection and radiation, as demonstrated in Figure 1C. Since the operation temperature in this situation is usually relatively low, the released adsorption heat will not affect the normal operation of devices. Considering the adsorption and desorption processes of the sorbent are temporally separate, the sorption-based evaporative cooling could also serve as a thermal storage system, i.e., thermal batteries.[55–57] The thermal storage capacity (Q, J) of the sorption-based evaporative cooling could be expressed as

$$Q = m_sH_{de}(W_l - W_h). \quad \text{(Equation 3)}$$

As shown in Figure 1C, the current storage level of the aforementioned adsorption-based thermal battery could be evaluated by the water content of the sorbent, and the adsorption and desorption could be analogized as charging and discharging processes, respectively. It should be mentioned that the thermal storage capacity of the proposed sorption-based evaporative cooling is sensitive to ambient RH, namely the ambient humidity ratio based on Figure 1D. Under the same temperature range between high and low workloads, a lower ambient humidity ratio will cause a smaller difference in RH and, finally, cause a smaller difference in water content based on Figure 1B. Nonetheless, considering the desorption enthalpy of sorption-based evaporative cooling is usually one order of magnitude larger than that of conventional solid-liquid phase-change materials (PCMs) at near room temperature,[34,58] the proposed passive cooling strategy is a promising one for regulation of the fluctuation workload and corresponding temperature of base stations.

Proof-of-concept experiment

As mentioned before, the performance of the proposed sorption-based evaporative cooling will be significantly affected by the property of sorption materials, such as the adsorption capacity and kinetics. After a comprehensive consideration including the cost, ease of fabrication, and working condition, the hygroscopic salt of LiCl and the matrix of ACF felt are considered and combined as the composite sorbent, which is further denoted as LiCl@ACF. Specifically, as demonstrated in Figure 1D, the adsorption of the sorbent might be operated under the condition of a low RH due to an operating temperature that is higher than ambient. Thus, the sorption capacity under low RH will play an important role in sorption-based evaporative cooling, where LiCl@ACF outperforms other materials.[50] Figure 2A demonstrates the sorbent preparation by the impregnation method. Specifically, the original ACF felt is immersed in LiCl solution with a mass concentration of 30%. The dried composite sorbent is repeatedly adsorbed under the maximum RH of subsequent experiments (i.e., 80%) until no leakage occurs to prevent potential leakage in the subsequent proof-of-concept experiment.[59] The leakage could also be completely avoided by hydrophobic encapsulations.[60] The scanning electron microscope (SEM) image, water sorption isotherms obtained by adsorption apparatus (ASAP 2020 plus) under 25°C, and thermogravimetric analysis coupled with differential scanning calorimetry (TGA-DSC) diagrams of the prepared sorbents are further evaluated and demonstrated in Figures 2B–2E and S1. Specifically, the results of isotherm curves demonstrate that the steady-state water uptakes under ambient RH conditions of 80%, 60%, and 40% are 3.31, 2.11, and 1.5 g g^{-1}, respectively, which are similar to literature.[50,53] The large gradient of the water sorption isotherms also increases the adaptability under different working conditions. That is, once the temperature and the corresponding RH difference exist, the adsorption/desorption cycles will occur. Besides, to avoid uncertainties, the TGA-DSC diagrams of two samples are measured by a simultaneous thermal analyzer (STA). Before measurement, all samples are placed in an environment-controlled chamber with an ambient condition of 25°C, RH 80%, for about 12 h. During the STA measurement, the steady-state temperature is set as 80°C, and the temperature

Please cite this article in press as: Liu et al., Passive thermal management of electronic devices using sorption-based evaporative cooling, Device (2023), https://doi.org/10.1016/j.device.2023.100122

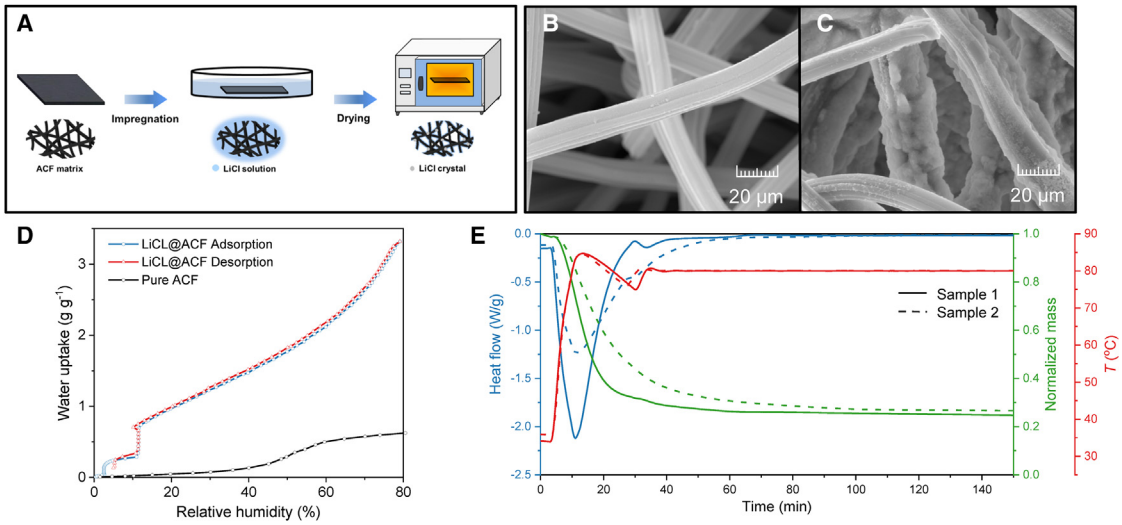

Figure 2. Preparation and characterization of the proposed LiCl@ACF composite sorbent

(A) Schematic illustration of sorbent fabrication.

(B) SEM images of pure ACF matrix.

(C) SEM images of LiCl@ACF composite sorbent.

(D) Water sorption isotherms of the pure ACF matrix and LiCl@ACF composite sorbent under an ambient condition of 25°C.

(E) TGA-DSC diagrams of the LiCl@ACF composite sorbent; two samples saturated under an ambient of 25°C, RH 80%, are measured.

fluctuation between 10 and 40 min shown in Figure 2E might be caused by the built-in temperature control algorithms. The obtained desorption enthalpies (per gram of desorbed water) of the two samples are about 2,424 and 2,386 J/g_{water}, respectively. Thus, an overall desorption enthalpy of 2,400 J/g_{water} is considered in the following analysis in this article.

To evaluate the performance of the proposed sorption-based evaporative cooling, the aforementioned LiCl@ACF composite sorbent is applied on an aluminum heat sink (hereinafter denoted as "with ACF"). The schematic illustration and photo of the proof-of-concept experiment are shown in Figures 3A and S2. Specifically, an electric heater is used to simulate the wasted heat generated by the inner power components of base stations. The electric heater is glued on the back side of the heat sink and further coved by a 20-mm-thick insulating form to ensure that most of the heat is dissipated through the heat sink. Besides, the structure and geometry of the heat sink are carefully designed based on a state-of-the-art base station with an overall dimension of about 60 × 32 × 65 mm (more details are in Figure S2). The heat sink contains three fins. For each fin, two cubic LiCl@ACF composite sorbents (60 × 30 × 2 mm) are closely attached on both sides and tightened by two strings, as shown in Figures 3A and 3B. Two thermocouples (denoted as *T1* and *T2*) and an infrared (IR) camera are considered to measure the temperature distribution of the heat sink, and the mass change of the heat sink with ACF is recorded by a precision electronic balance. For comparison, the same experimental setup is implemented on another heat sink with bare surfaces (without ACF, hereinafter denoted as "baseline"). A more detailed description of the experimental procedure is demonstrated in Note S1. All experiments are implemented on an environment-controlled chamber, and the corresponding ambient temperature and RH are demonstrated in Figure S5.

The cooling performance of the proposed sorption-based evaporative cooling is first tested under a 15 W constant workload, as shown in Figures 3, S3, and S4. Specifically, to comprehensively evaluate the influence of ambient RH, the experiment is conducted under three ambient RH conditions, i.e., 80%, 60%, and 40%. The results show that, compared with the baseline, the LiCl@ACF composite sorbent could bring about significant temperature reduction (i.e., the temperature difference at the same location between the heat sink with ACF and the baseline) of the whole system until the stored water is exhausted. As demonstrated in Figure 3C, the temperature reduction of two monitor points (*T1* and *T2*) is almost the same, showing that not only the surface of the heat sink but also the heat source are effectively cooled. The IR images shown in Figure 3B clearly demonstrate the strong cooling effect of the proposed sorption-based evaporative cooling and also prove the good contact between the LiCl@ACF composite sorbent and the heat sink. The maximum temperature reductions between the heat sink with ACF and the baseline for ambient RH conditions of 80%, 60%, and 40% are about 20.4°C, 12.7°C, and 9.8°C, respectively. The mass change of the sorbent during the 3-h high-workload period is demonstrated in Figure 3E, and a corresponding analysis based on the linear driving force (LDF) model is demonstrated in Note S2. The maximum mass losses under the aforementioned three ambient RH conditions are about 13.7, 8.4, and 6.1 g. Considering the total mass of the LiCl@ACF composite sorbent attached to the heat sink is about 5.1 g (including the strings), the water uptake of the sorbent on heat sinks is a little lower than that of the samples measured by ASAP. The average cooling capacity of the sorption-based evaporative cooling (q_{de}, W·m^{-2}) could be calculated by[24]

Please cite this article in press as: Liu et al., Passive thermal management of electronic devices using sorption-based evaporative cooling, Device (2023), https://doi.org/10.1016/j.device.2023.100122

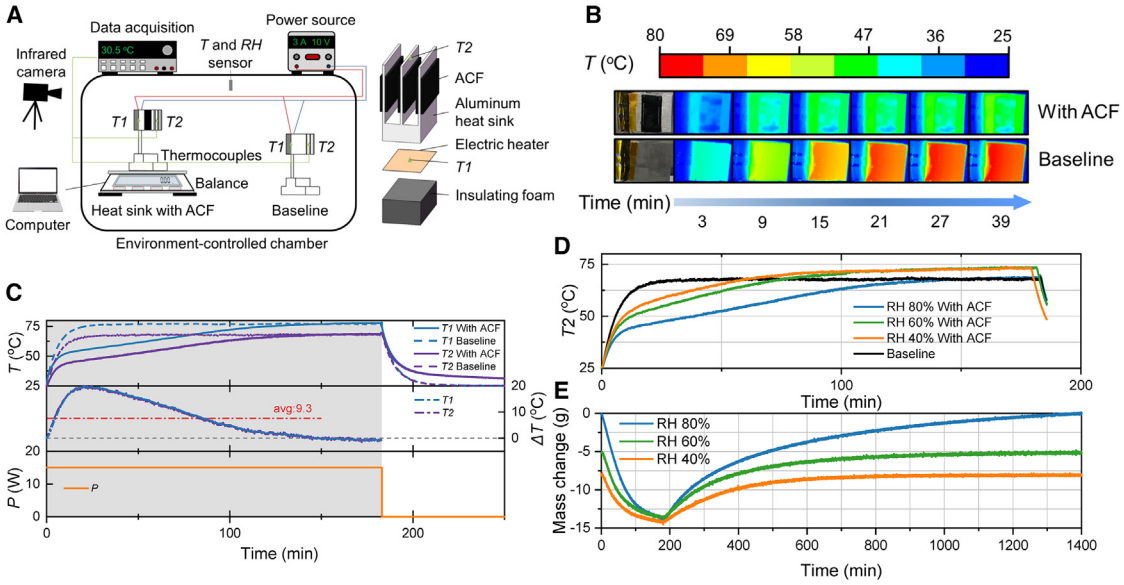

Figure 3. Proof-of-concept experiment under the constant workload

(A) Schematic illustration of the experimental setup.

(B) IR images of exterior surfaces after a fixed time sample under an ambient RH of 80%.

(C) Transient temperature (T) of monitor points, temperature difference (ΔT) between the heat sink with ACF and baseline, and workload (P) under an ambient RH of 80%.

(D) Transient temperature distribution of monitor point $T2$ under different ambient RH conditions.

(E) The corresponding mass change of LiCl@ACF composite sorbent under different ambient RH conditions.

$$q_{de} = \frac{H_{de} \times \Delta m_s}{t \times A}, \qquad \text{(Equation 4)}$$

where Δm_s represents the mass change of the LiCl@ACF composite sorbent. For the 3-h operation under three different ambient RH conditions, the average cooling capacities are about 281, 172, and 125 W/m^2, respectively.

Considering the attachment of the LiCl@ACF composite sorbent will also bring about an extra thermal conductive resistance, the application of sorption-based evaporative cooling will also inevitably bring about a negative impact after the stored water is almost exhausted. As demonstrated in Figure 3D, the effective times, which are defined as the time duration when the temperature of the heat sink with ACF is lower than that of the baseline, of three ambient RH conditions are about 150, 70, and 60 min. During the effective time, the average temperature reductions of sorption-based evaporative cooling of three ambient RH conditions are about 7.6°C, 6.9°C, and 5.6°C, respectively. Finally, after a 3-h long-term operation, the temperatures of the heat sink with ACF under three ambient RH conditions are about 1°C, 5°C, and 5°C higher than that of the baseline. To avoid the negative impact caused by sorption-based evaporative cooling, a more comprehensive co-design between the effective time and the duration of the peak workload could be considered.

To demonstrate a deeper analysis of the proposed sorption-based evaporative cooling, a computational fluid dynamic (CFD) simulation is conducted based on ANSYS Icepak. Specifically, the transient equivalent cooling capacity of the sorbent is calculated based on Equation 4 and is further approximated as a surface cooling source term at the interface between the sorbent and the heat sink.[61] The detailed simulation setup and corresponding thermal properties[62] are demonstrated in Note S2 and Table S1, respectively. The results show that the proposed CFD model has good accuracy compared with the experiment. The transient deviation between the simulation and experimental results is within 10% in both the baseline and the heat sink with ACF. The comparison of temperature distribution obtained from the IR camera and the CFD model is further presented in Figures S7 and S8. The simulated temperature is slightly higher than that of the experimental results partly due to the minor air disturbance caused by the inner fan of the environment-controlled chamber, which is not considered in the CFD simulation. A heat flow analysis is further conducted based on the proposed CFD model as demonstrated in Figures 4B and 4D. In the baseline, about 95% of the total power (15 W) is dissipated through the heat sink, and the remaining power is transferred through the insulating form. Of the heat flow transferred through the heat sink, about 29% is dissipated by heat radiation, and the remaining heat flow is transferred to the ambient by natural convection. It should be mentioned that since the heat flow of the natural convection is calculated by the difference between the total heat flow transferred through the heat sink and that of the radiation, it might be slightly exaggerated at the beginning due to the influence of thermal capacity. The steady-state heat transfer coefficient of the natural convection is about 12.8 W m^{-2}·K^{-1}. A transient heat flow analysis of the heat sink with ACF is then demonstrated in Figure 4D. Due to the application

Please cite this article in press as: Liu et al., Passive thermal management of electronic devices using sorption-based evaporative cooling, Device (2023), https://doi.org/10.1016/j.device.2023.100122

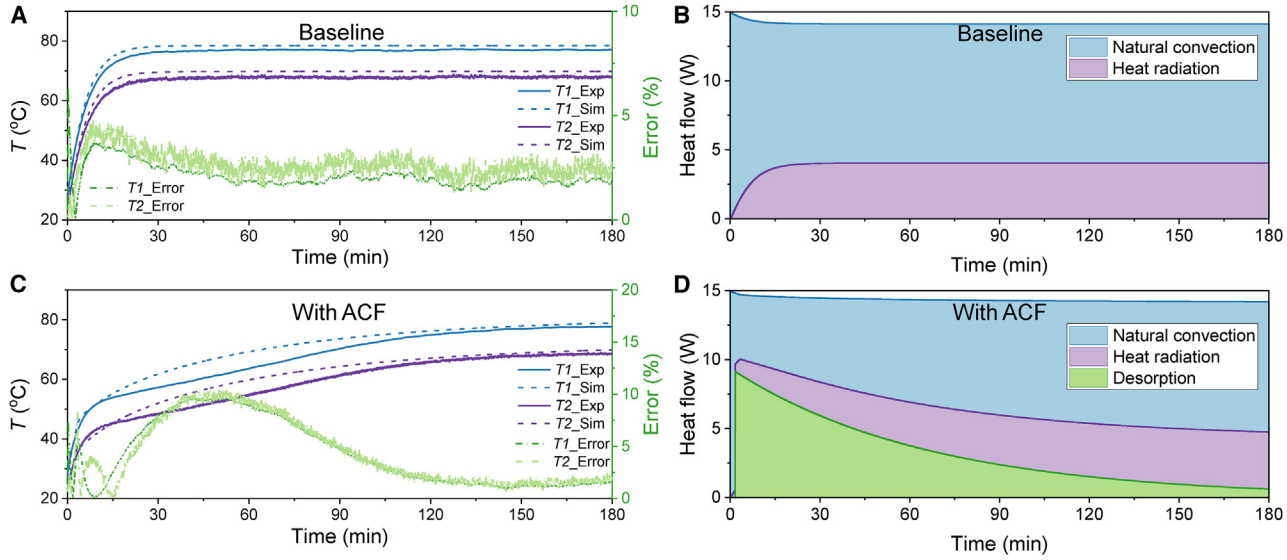

Figure 4. CFD simulation results of the proof-of-concept experiment

(A) Comparison of experimental and simulation results for baseline.

(B) Heat flow analysis for baseline.

(C) Comparison of experimental and simulation results for heat sink with ACF.

(D) Heat flow analysis for heat sink with ACF.

of sorption-based evaporative cooling, on average, about 22% and 23% of the heat transferred through the heat sink are dissipated by the desorption and the heat radiation, respectively, and the steady-state heat transfer coefficient of the natural convection is about 11.7 W $m^{-2}\cdot K^{-1}$.

Since the practical base station is usually operated under a transient workload—i.e., a stable peak in a day and a low workload during the remaining time—the cooling performance of the proposed sorption-based evaporative cooling is then evaluated under the intermittent workload. In the proof-of-concept experiment, the high workload lasts about 40 min (i.e., discharging), while the low workload lasts about 160 min for recovery (i.e., charging). Namely, the ratio of desorption and recovery duration is kept at 1:4. To comprehensively evaluate the proposed cooling strategy under different working conditions, three different ambient RH conditions, 80%, 60%, and 40%, and different power consumption under the recovery process, i.e., different adsorption temperatures, are considered, as shown in Figure 5. In Figure 5A, the cooling effect under a 15-0 W cyclic workload with an ambient RH of 80% is demonstrated. As mentioned before, the water content of the sorbent could represent the remaining cooling capacity of the thermal battery; thus, the results show that the LiCl@ACF composite sorbent is not completely recovered in 160 min. The cooling performance of three high-low workload cycles is gradually degraded. The average temperature reductions under the 40-min high-workload duration of three cycles are about 16.1°C, 11.6°C, and 10.4°C, respectively. The mass losses of the sorbent of three cycles are about 6.5, 4.9, and 4.4 g, respectively, which correspond to equivalent average cooling capacities of 602, 435, and 306 W/m^2, respectively. The temperature of the heat sink with ACF is slightly higher than that of the baseline in the recovery period due to the exothermic adsorption process. Furthermore, the mass change of a longer timescale is demonstrated in Figure S6. The results show that the system could achieve sustainable operation (i.e., balance between charging and discharging) under the working condition of the last cycle if an about 10-min-longer recovery time is considered.

The cooling performance under the 15-4-15-2.5 W transient workload with an ambient RH of 80% is demonstrated in Figure 5B. As demonstrated in Figure 1D, when the adsorption process is operated under a relatively low workload, the equilibrium RH and the corresponding water sorption capacity of the sorbent will decrease, which will further cause a performance deterioration of both the thermal storage and the cooling. In the first low workload duration (40–200 min in Figure 5B), since the remaining water content after the 40-min desorption is still higher than the equilibrium point under the temperature conditions, the desorption process, rather than the adsorption process, occurs. The average temperature reductions under the 40-min high-workload duration of three cycles are about 16.2°C, 4.7°C, and 5.1°C, respectively. The mass losses of the sorbent of three cycles are about 6.5, 2.9, and 3 g, which correspond to equivalent average cooling capacities of 602, 269, and 278 W/m^2, respectively. The mass change of the sorbent also illustrates that the system could achieve a sustainable operation under the working condition of the last cycle since the sorbent could adsorb about 3 g water from the ambient in 160 min with a power consumption of 2.5 W. Finally, the cooling effect under the 15-0-15-2.5 W transient workload with ambient RH conditions of 60% and 40% is demonstrated in Figures 5C and 5D. Similar to previous results, the low ambient RH will bring about a negative impact on the cooling performance, and the average temperature reduction will also decrease due to incomplete recovery. Nonetheless, the

Please cite this article in press as: Liu et al., Passive thermal management of electronic devices using sorption-based evaporative cooling, Device (2023), https://doi.org/10.1016/j.device.2023.100122

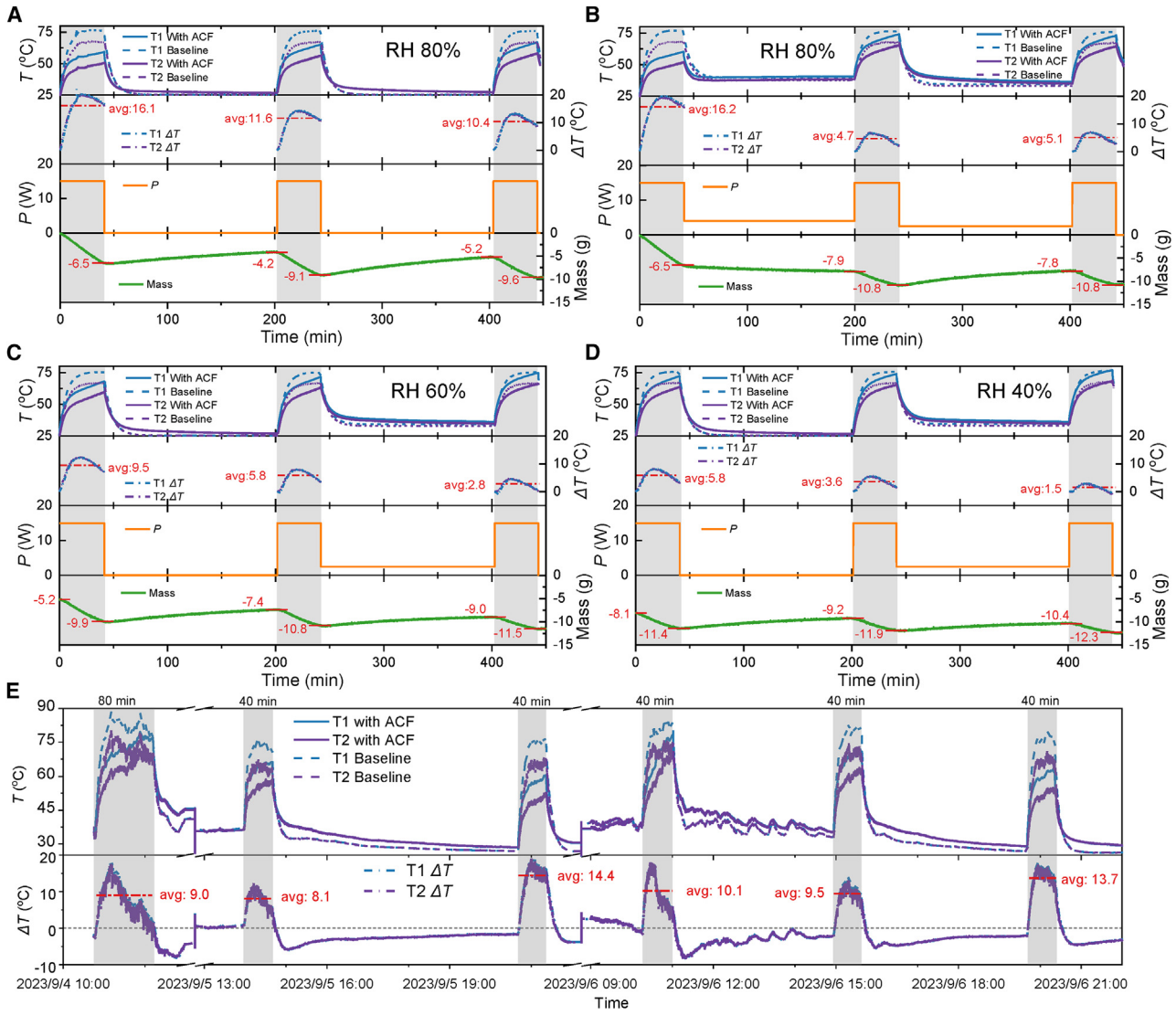

Figure 5. Proof-of-concept experiment under intermittent workload

(A) The transient *T* of monitor points, *ΔT* between the heat sink with ACF and baseline, intermittent *P*, and mass change of LiCl@ACF composite sorbent under an ambient RH of 80%, with a zero low workload.

(B) Cooling performance under an ambient RH of 80%, with non-zero low workload.

(C) Cooling performance under an ambient RH of 60%.

(D) Cooling performance under an ambient RH of 40%.

(E) Outdoor experiment under 15-0 W transient workload.

sorption-based evaporative cooling could still bring about a 2°C–3°C temperature reduction even in the worst cases. The equivalent cooling capacities of the first cycle under ambient RH conditions of 60% and 40% are about 435 and 306 W/m^2, respectively.

To further demonstrate the feasibility of the proposed sorption-based evaporative cooling, an outdoor experiment was conducted continuously for 3 days. The experimental setup and ambient conditions are demonstrated in Figures S9 and S10, respectively. Specifically, a 15-0 W transient workload with different adsorption durations is tested. As shown in Figure 5E, the results demonstrate that the proposed cooling method could bring about an 8°C–14°C average temperature reduction compared with the baseline situation in outdoor conditions. It should be mentioned that outdoor wind will increase both the desorption and adsorption rates, and the relatively high RH during the night time will also be helpful for adsorption. Meanwhile, although the sunlight will increase the surface temperature, the relatively high RH also provides the possibility for adsorption. As a result, the outdoor experiment could achieve similar and even better results compared with that of the indoor experiment.

Demonstration on a state-of-the-art base station

To further evaluate the cooling performance of the proposed sorption-based evaporative cooling, the proposed sorption

Please cite this article in press as: Liu et al., Passive thermal management of electronic devices using sorption-based evaporative cooling, Device (2023), https://doi.org/10.1016/j.device.2023.100122

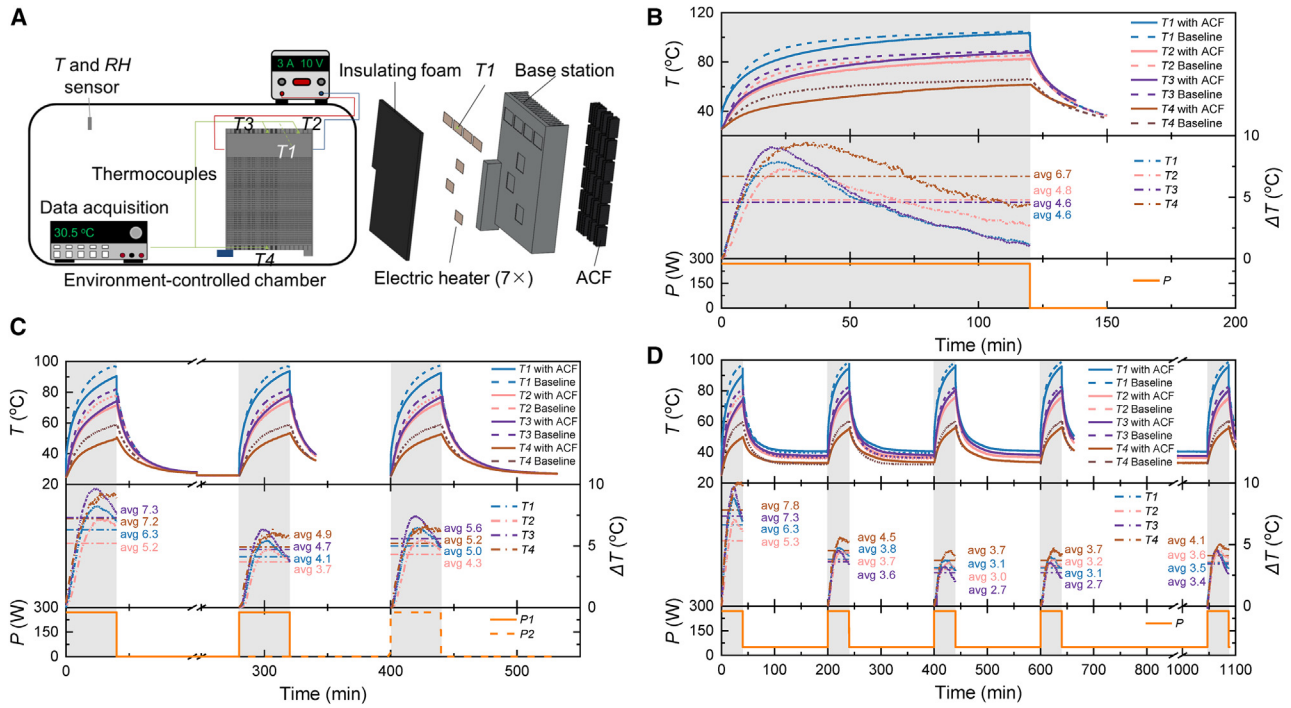

Figure 6. Demonstration on a state-of-the-art base station

(A) Schematic illustration of the experimental setup.

(B) Cooling performance under a 270 W constant workload.

(C) Cooling performance with different adsorption durations under zero power consumption.

(D) Cooling performance under a 270-50 W intermittent workload.

material, i.e., LiCl@ACF, is applied on a state-of-the-art base station. The experimental setup and photo are demonstrated in Figures 6A and S11, respectively. Specifically, seven electronic heaters are carefully connected with wires and then sandwiched between the back side of the base station and the thermal insulating form to simulate the power components (e.g., chips). Since the enclosure and fins on the state-of-the-art base station are carefully designed and optimized, the inner structure of the base station is extremely complicated and irregular. As a result, after comprehensive consideration, only eight of the eighteen fins are covered by the sorption materials, to achieve good contact between the sorbent and the surface of fins. For both sides of the fins with sorption materials, six cubic LiCl@ACF composite sorbents are connected in series by two strings, as demonstrated in Figure S11. Considering about 90-mm-height water could be vertically held in the pores of ACF by its strong capillary force,[50] the height of the cubic LiCl@ACF composite sorbents here is determined as 60 mm to prevent leakage. Four thermocouples (denoted as *T1* to *T4*) are considered to comprehensively monitor the temperature profile of the base station. In particular, the monitor points of *T1* to *T4* respectively record the temperature of the heat source (electric heater), the upper side of fins without ACF, the upper side of fins with ACF, and the lower side of fins with ACF. For comparison, the same workload is re-implemented on the same base station without the LiCl@ACF composite sorbents (denoted as baseline). All experiments are implemented on an environment-controlled chamber, and the corresponding ambient temperature and RH are demonstrated in Figure S12.

The cooling performance of the proposed cooling strategy under a constant high workload within 2 h is first evaluated, as shown in Figure 6B. The whole experiment is conducted under an ambient condition of 25°C, 80% RH. Before the experiment, both the baseline and the base station with ACF are placed under the ambient condition for more than 12 h. The results show that during this long-lasting high workload, the proposed cooling strategy could distinctly reduce the temperature of the whole base station. The average and maximum temperature reductions of the four monitor points are about 5°C–7°C and 8°C–10°C, respectively. The temperature profile of the base station has a spatially uneven distribution due to the floorplan of heat sources, thus causing a different temperature reduction of the four monitor points. It should be mentioned that not only the temperature of fins with ACF (*T3* and *T4*) but also the temperature of the heat source and fins without ACF (*T1* and *T2*) are reduced, which demonstrates that the whole base station is cooled by the proposed cooling strategy. Meanwhile, since the commercial base station has been extensively designed and optimized and almost reaches the heat dissipation bottleneck caused by the natural convection and radiation, any further improvement is extremely difficult and valuable. Furthermore, considering the risk of potential damage to electric heaters under long-lasting operation with high temperatures, a longer operation duration is thus not explored. And the effective time could be approximately determined as more than 120 min since

Please cite this article in press as: Liu et al., Passive thermal management of electronic devices using sorption-based evaporative cooling, Device (2023), https://doi.org/10.1016/j.device.2023.100122

the temperature of the baseline is still higher than that of the base station with ACF at the end of the 2-h experiment.

The cooling performance under intermittent workload, i.e., different incomplete recovery conditions, is further evaluated. In specific, Figure 6C demonstrates the cooling performance with different recovery (i.e., charging) times under the power consumption of zero. After a 40-min 270 W high workload (i.e., discharging) process, the cooling performances of another round of 40-min high workloads after 240 and 360 min adsorption durations are measured. The results show that incomplete recovery will result in performance deterioration. The average temperature reduction within the first round of the 40-min high workload (i.e., fully recovered) is about 5.2°C–7.3°C, while those of the second round of the 40-min high workload after 240 and 360 min adsorption durations are about 3.7°C–4.9°C and 4.3°C–5.6°C, respectively. Figure 6D demonstrates the cooling performance when the power consumption of 50 W is considered in the recovery process. In the first four high-low workloads cycles, the discharging and charging durations are determined to be 40 and 160 min, respectively, while in the last round of the 40-min high workload, the cooling performance after a 400-min adsorption process is evaluated. The results demonstrate that the proposed cooling strategy could still bring appreciable cooling effects under such adverse adsorption conditions. Under the aforementioned cyclic high-low workload, the average temperature reduction will gradually decrease from the beginning 5.3°C–7.8°C to 2.7°C–3.7°C and then achieve a sustainable operation. Then, after long-term (400 min) adsorption under the power consumption of 50 W, the temperature reduction could then slightly increase to 3.4°C–4.1°C.

In summary, the application of sorption-based evaporative cooling on the practical base station could generally bring about a 5°C–8°C temperature reduction of the surface temperature. On one hand, temperature reduction has great benefits for the reliability of electronics. It is estimated that for every 10°C rise in temperature, the average reliability will be decreased by 50%. On the other hand, assuming the surface temperature of original devices is about 70°C under a 270 W power consumption. The temperature reduction of 5°C–8°C is equivalent to a 13%–21% increase in power consumption (i.e., performance) when keeping the same surface temperature. The aforementioned results comprehensively evaluate the cooling performance under different working conditions and thus demonstrate the wide applicability of the proposed cooling strategy.

DISCUSSION

Evaluation criteria and comparison with representative studies

As an emerging cooling strategy, sorption-based evaporative cooling is still at its very early stage of development.[63] Thus, uniform evaluation criteria for comparisons between different devices and systems are still absent. A comprehensive comparison under multiple indexes of the proposed cooling strategy with the existing work is demonstrated in Table 1. Among them, the most intuitive index is the temperature reduction after utilizing the sorption-based evaporative cooling compared with the original system. As demonstrated in Table 1, the temperature reduction of the proposed system, either the maximum or the average, altogether outperforms most of the existing works. However, pure temperature reduction cannot reflect the overall cooling performance of the sorption-based evaporative cooling since different devices have different backgrounds and working conditions. For instance, if the heat transfer structure of the baseline device is well designed, any further heat transfer enhancement is difficult and thus will naturally result in a relatively small temperature reduction. Meanwhile, considering the temperature reduction is generally evaluated in a transient heating process, the average temperature reduction during the effective time might be more suitable than the maximum temperature reduction to avoid uncertainties and thus demonstrate the overall cooling performance. Furthermore, it should be mentioned that the temperature of the exterior surface, which could be easily measured by an IR camera, might be inappropriate to directly adopt in the calculation of temperature reduction. Compared with the original bare surface, the outer surface temperature of the sorbent materials will naturally decrease no matter whether desorption occurs since an extra conductive thermal resistance is involved. Namely, directly using the temperature obtained from the IR camera might make the temperature reduction exaggerated.

The average cooling capacity of the proposed sorption-based evaporative cooling in different working conditions is further demonstrated in Table 1. It should be mentioned that in many previous studies, the average cooling capacity is absent, and thus the specific values are secondarily calculated based on their experimental results through Equation 4. Although the equivalent cooling capacity is still influenced by the working conditions, e.g., a higher operating temperature usually leads to a faster desorption rate and, finally, results in a larger equivalent cooling capacity, it might be more suitable to serve as a representative evaluation index since it combines the key parameters of the sorption-based evaporative cooling, including the desorption dynamics and enthalpy. Meanwhile, the dimension of the equivalent cooling capacity (W, or W/m^2) makes it more convenient for comparison between different cooling strategies, such as convection and radiation, and also more straightforward to thermal engineers. Furthermore, governed by Equation 2, in general, the desorption rate is relatively fast when the water content of the sorbent is high. Namely, once the adsorption-based thermal battery is fully charged before discharge, the average cooling capacity of the first several minutes will be larger than that of the whole complete discharge process. Thus, both the operating temperature and the water content state of the sorbent should be considered when evaluating the average cooling capacity between different devices and systems. Since the working condition in this article is not the same as those of the previous studies, it is hard to quantitatively evaluate the improvement from the perspective of cooling capacity. However, the proposed cooling strategy generally outperforms the existing works partly due to the good heat transfer design and low mass transfer resistance. For instance, compared to literature,[21] where the highest cooling capacity of previous works is obtained, the proposed cooling strategy could achieve a 6% improvement in cooling capacity under worse working conditions, such as lower desorption temperature and longer desorption duration.

Please cite this article in press as: Liu et al., Passive thermal management of electronic devices using sorption-based evaporative cooling, Device (2023), https://doi.org/10.1016/j.device.2023.100122

Table 1. Comparison of the proposed sorption-based evaporative cooling with representative studies

	Sorbent material	Object	Ambient		Operating	Cooling effect			Mass of the sorbent (g)			Ev/Ad duration	H_{de} (J/g_{water})	Cost of sorbent (USD/kg)
			T_a (°C)	RH (%)	T (°C)	ΔT avg (°C)	ΔT max (°C)	q_{de} (W/m^2)	Dry	Δm_s	Saturated			
This work	LiCl@ACF	base station	25	80, 60, 40	50–60	9.3, 6.9, 5.6	20, 12.7, 9.8	282/602, 173/435, 126/306	5.1	13.7/6.5, 8.4/4.7, 6.1/3.3	18.8, 13.5, 11.2	3/20 h, 3/13 h, 3/10 h	2,400	~10
Wang et al.[34]	MIL-101(Cr)	chip	25	60	~55	N/A	8.6	190–240	0.124–0.288	0.081–0.243	0.205–0.531	20/60 min	2,400	>100,000
Xu et al.[37]	MIL-101(Cr)@CF	battery	30	60	40–50	N/A	8.3	32–40	0.51	0.357	0.867	100–130/130–137 min	2,541	>100,000
Li et al.[24]	PAM-CNT-CaCl2	PV	22	60	50	10–15	10–15	250–330	6.2	2.75–3.65	11	11/17 h	2,450	N/A
Pu et al.[21]	Li-PAAm hydrogel	PV	30	40	50	13–17	13–17	144	N/A	13	42	6/10 h	N/A	N/A
Pu et al.[21]	Li-PAAm hydrogel	chip	25	70	80	N/A	15.2	570	N/A	0.13	1.13	12/70 min		
Pu et al.[38]	thermogalvanic hydrogel	battery	26	80	50	N/A	20	218	N/A	0.4	2.65	1.7/5.88 h	N/A	NA
Li et al.[20]	PAm/alginate-CaCl2	PV	30	75	45–55	3.5	7.5	140	25.5	11.5	45.5	12/12 h	N/A	2.68
Zeng et al.[33]	[P(SA)] hydrogel	chip	22	85 (Ad), 60 (Ev)	30–35	N/A	~8	34.6	27.2	15.5	51.7	3/12 h	2,300	~2

A default desorption enthalpy of 2,400 J/g_{water} is considered where its specific value is absent. Ad, adsorption; Ev, evaporation.

Limitations and future works

In Note S1, it has been demonstrated that the proposed cooling strategy will not naturally exhibit the cooling effect for every system unless certain criteria are satisfied. Besides the thermal design, the effectiveness of the proposed cooling strategy will also be influenced by the sorbent performance and ambient conditions. In particular, the proposed cooling strategy will achieve its best performance (i.e., upper limit) when the sorbent is saturated, and then the equivalent cooling power will gradually decrease, as demonstrated in Equation 2 and Figure 4. The saturation state of the sorbent will be affected by the adsorption condition, including ambient condition, power consumption of low-workload period, and duration of low-workload period. To achieve better performance, a higher ambient RH, near-zero power consumption of low-workload period, and longer adsorption duration are preferred. In the current situation, although the adsorption (recovery) rate is relatively slow, the proposed cooling strategy could still meet the requirement of some specific base stations whose peak hours are more compact, such as devices near meeting rooms and stadiums. The system (or material) with a shorter ratio of adsorption and desorption duration is expected in the future.

Cycle stability is another main concern of the sorption-based techniques. For the sorbent material used in this article, its cycle stability has been proven in previous literature.[53,60] In our experiment, about thirteen cycles were conducted in the proof-of-concept experiment, and nine cycles were carried out in the practical base station experiment. Nonetheless, considering the proposed cooling strategy is mainly operated outside, hydrophobic encapsulations or physical structures could be considered to prevent the scouring of rainwater. Furthermore, different from the other moisture-adsorption-based techniques, the co-design among the storage capacity (i.e., sorbent mass, adsorption capacity, and enthalpy), adsorption/desorption kinetics, workloads, and ambient conditions is more critical for achieving the practical and sustainable application of the sorption-based evaporative cooling.

EXPERIMENTAL PROCEDURES

Resource availability

Lead contact

Further information and requests for additional details should be directed to and will be fulfilled by the lead contact, Prof. Ruzhu Wang (rzwang@sjtu.edu.cn).

Materials availability

This study did not generate new unique reagents.

Data and code availability

All data needed to evaluate the conclusions in this article are present in the paper and/or the supplemental information and are available from the lead contact upon reasonable request.

Synthesis of LiCL@ACF composite sorbent

The ACF felt with a thickness of about 2 mm (purchased from Jiangsu Kejing Carbon Fiber Company) is cut into specific shapes and then immersed into the LiCl (98%, purchased from Innochem) solution with a mass concentration of 30% for about 12 h. Then, the samples are dried at 90°C for about 8 h. The obtained sorbent is repeatedly adsorbed in a constant climate chamber (BINDER) for about 12 h with an ambient of 25°C, RH 80%, until no leakage occurs after 12-h adsorption.

Characterization

The obtained LiCL@ACF composite sorbent is observed by scanning electron microscopy (VEGA 3, TESCAN) operating at 20.0 kV. The TGA-DSC diagram of the sorbent is measured by the STA device (STA 499, NETZSCH) equipped with a humidity generator. Before the measurement, the samples are fully saturated under an ambient of 25°C, RH 80%. An about 30-mg sample is put inside the measurement chamber. The measurement starts at a temperature lifting rate of 5 K/min from the room temperature to about 80°C and is then kept at 80°C for about 120 min. The variations of mass and heat flow rate are tested with accuracies of 0.1 μg and 1 μW, respectively. The water sorption isotherms of the sorbents are measured by an adsorption apparatus (ASAP 2020 plus, Micromeritics) with the addition of a water vapor generator, a jacketed beaker, and a constant temperature water bath. These additional components together precisely control and adjust the temperature and RH of the test chamber.

Experimental setup

The aforementioned sorbent is attached to an aluminum heat sink (in the proof-of-concept experiment) fabricated by the computer numeric control (CNC) machine and a practical heat sink of 5G base station on both sides of the fins and is tightened by two strings. K-type thermocouples (TT-K-40-SLE, Omega) with an ultra-thin wire (80 μm in diameter) and an IR camera (T630sc, FLIR, with an accuracy of ±1°C) are employed to measure the thermal profile. The thermocouples are pre-calibrated with an accuracy of 0.1 K before experiments and connected to a data logger (TP700, TOPRIE). The mass change of test devices is recorded by a precision electronic balance (ME503TE, METTLER TOLEDO) with a resolution of 1 mg, which is in real-time communication with the computer. All experiments are conducted in a constant climate chamber (BINDER), and the ambient condition is measured by a thermo-hygrometer sensor (COS-4, Renke).

The outdoor experiment was continuously conducted on the roof of the Sino-Italy Green Energy Laboratory at Shanghai Jiao Tong University, China, from September 4th to 6th, 2023. The temperature is measured by the aforementioned thermocouples. Other ambient data are collected from a portable meteorological station (YGC-BYX-M, YIGU).

SUPPLEMENTAL INFORMATION

Supplemental information can be found online at https://doi.org/10.1016/j.device.2023.100122.

ACKNOWLEDGMENTS

The authors thank the members of ITEWA (Innovative Team for Energy Water and Air) of Shanghai Jiao Tong University (SJTU) for their discussions and suggestions. This research work was founded by the Fundamental Research Funds for the Central Universities and the Foundation for Innovative Research Groups of the National Natural Science Foundation of China (no. 51521004).

AUTHOR CONTRIBUTIONS

H.L. conceived the concept of this work under the supervision of R.W. H.L., J.Y., and C.W. designed and conducted the experiments. H.L., Z.Z., and P.P. implemented the CFD simulation and helped with the mechanism discussion and data analysis. R.W. led this research. All authors contributed to writing and revising the paper.

DECLARATION OF INTERESTS

The authors declare no competing interests.

INCLUSION AND DIVERSITY

We support inclusive, diverse, and equitable conduct of research.

Received: July 26, 2023
Revised: September 27, 2023
Accepted: October 3, 2023
Published: October 31, 2023

REFERENCES

1. van Erp, R., Soleimanzadeh, R., Nela, L., Kampitsis, G., and Matioli, E. (2020). Co-designing electronics with microfluidics for more sustainable cooling. Nature *585*, 211–216. https://doi.org/10.1038/s41586-020-2666-1.
2. Zhang, Q., Deng, K., Wilkens, L., Reith, H., and Nielsch, K. (2022). Micro-thermoelectric devices. Nat. Electron. *5*, 333–347. https://doi.org/10.1038/s41928-022-00776-0.
3. Kang, J.S., Li, M., Wu, H., Nguyen, H., Aoki, T., and Hu, Y. (2021). Integration of boron arsenide cooling substrates into gallium nitride devices. Nat. Electron. *4*, 416–423. https://doi.org/10.1038/s41928-021-00595-9.
4. Pagani, S., Manoj, P.D.S., Jantsch, A., and Henkel, J. (2020). Machine Learning for Power, Energy, and Thermal Management on Multicore Processors: A Survey. IEEE Trans. Comput. Aided Des. Integrated Circ. Syst. *39*, 101–116. https://doi.org/10.1109/tcad.2018.2878168.
5. Liu, H.R., Wang, C.X., Li, B.J., Hua, L.J., Yu, J.Q., and Wang, R.Z. (2022). Reversible sweat cooling on mobile electronic devices by metal-organic frameworks-based moisture sorption-desorption process. Materials Today Nano *18*, 100198. https://doi.org/10.1016/j.mtnano.2022.100198.
6. Mytton, D., and Ashtine, M. (2022). Sources of data center energy estimates: A comprehensive review. Joule *6*, 2032–2056. https://doi.org/10.1016/j.joule.2022.07.011.
7. Abbas, A., and Wang, C.-C. (2020). Augmentation of natural convection heat sink via using displacement design. Int. J. Heat Mass Tran. *154*, 119757. https://doi.org/10.1016/j.ijheatmasstransfer.2020.119757.
8. Joo, Y., Lee, I., and Kim, S.J. (2018). Efficient three-dimensional topology optimization of heat sinks in natural convection using the shape-dependent convection model. Int. J. Heat Mass Tran. *127*, 32–40. https://doi.org/10.1016/j.ijheatmasstransfer.2018.08.009.
9. Gebrael, T., Li, J., Gamboa, A.R., Ma, J., Schaadt, J., Horowitz, L., Pilawa-Podgurski, R., and Miljkovic, N. (2022). High-efficiency cooling via the monolithic integration of copper on electronic devices. Nat. Electron. *5*, 394–402. https://doi.org/10.1038/s41928-022-00748-4.
10. Zeng, S., Pian, S., Su, M., Wang, Z., Wu, M., Liu, X., Chen, M., Xiang, Y., Wu, J., Zhang, M., et al. (2021). Hierarchical-morphology metafabric for scalable passive daytime radiative cooling. Science *373*, 692–696. https://doi.org/10.1126/science.abi5484.
11. Yin, X., Yang, R., Tan, G., and Fan, S. (2020). Terrestrial radiative cooling: Using the cold universe as a renewable and sustainable energy source. Science *370*, 786–791. https://doi.org/10.1126/science.abb0971.
12. Zhang, Y., Nandakumar, D.K., and Tan, S.C. (2020). Digestion of Ambient Humidity for Energy Generation. Joule *4*, 2532–2536. https://doi.org/10.1016/j.joule.2020.10.003.
13. An, S., Shi, B., Jiang, M., Fu, B., Song, C., Tao, P., Shang, W., and Deng, T. (2023). Biological and Bioinspired Thermal Energy Regulation and Utilization. Chem. Rev. *123*, 7081–7118. https://doi.org/10.1021/acs.chemrev.3c00136.
14. Feng, C., Yang, P., Liu, H., Mao, M., Liu, Y., Xue, T., Fu, J., Cheng, T., Hu, X., Fan, H.J., and Liu, K. (2021). Bilayer porous polymer for efficient passive building cooling. Nano Energy *85*, 105971. https://doi.org/10.1016/j.nanoen.2021.105971.
15. Lu, Z., Strobach, E., Chen, N., Ferralis, N., and Grossman, J.C. (2020). Passive Sub-Ambient Cooling from a Transparent Evaporation-Insulation Bilayer. Joule *4*, 2693–2701. https://doi.org/10.1016/j.joule.2020.10.005.
16. Xu, L., Sun, D.W., Tian, Y., Sun, L., Fan, T., and Zhu, Z. (2022). Combined Effects of Radiative and Evaporative Cooling on Fruit Preservation under Solar Radiation: Sunburn Resistance and Temperature Stabilization.

ACS Appl. Mater. Interfaces *14*, 45788–45799. https://doi.org/10.1021/acsami.2c11349.

17. Xu, L., Sun, D.-W., Tian, Y., Fan, T., and Zhu, Z. (2023). Nanocomposite hydrogel for daytime passive cooling enabled by combined effects of radiative and evaporative cooling. Chem. Eng. J. *457*, 141231. https://doi.org/10.1016/j.cej.2022.141231.
18. Li, J., Wang, X., Liang, D., Xu, N., Zhu, B., Li, W., Yao, P., Jiang, Y., Min, X., Huang, Z., et al. (2022). A tandem radiative/evaporative cooler for weather-insensitive and high-performance daytime passive cooling. Sci. Adv. *8*, eabq0411. https://doi.org/10.1126/sciadv.abq0411.
19. Lu, Z., Leroy, A., Zhang, L., Patil, J.J., Wang, E.N., and Grossman, J.C. (2022). Significantly enhanced sub-ambient passive cooling enabled by evaporation, radiation, and insulation. Cell Reports Physical Science *3*, 101068. https://doi.org/10.1016/j.xcrp.2022.101068.
20. Li, Z., Ma, T., Ji, F., Shan, H., Dai, Y., and Wang, R. (2023). A Hygroscopic Composite Backplate Enabling Passive Cooling of Photovoltaic Panels. ACS Energy Lett. *8*, 1921–1928. https://doi.org/10.1021/acsenergylett.3c00196.
21. Pu, S., Fu, J., Liao, Y., Ge, L., Zhou, Y., Zhang, S., Zhao, S., Liu, X., Hu, X., Liu, K., and Chen, J. (2020). Promoting Energy Efficiency via a Self-Adaptive Evaporative Cooling Hydrogel. Adv. Mater. *32*, e1907307. https://doi.org/10.1002/adma.201907307.
22. Gkaniatsou, E., Meng, B., Cui, F., Loonen, R., Nouar, F., Serre, C., and Hensen, J. (2021). Moisture-participating MOF thermal battery for heat reallocation between indoor environment and building-integrated photovoltaics. Nano Energy *87*, 106224. https://doi.org/10.1016/j.nanoen.2021.106224.
23. Mu, X., Shi, X.-L., Zhou, J., Chen, H., Yang, T., Wang, Y., Miao, L., and Chen, Z.-G. (2023). Self-hygroscopic and smart color-changing hydrogels as coolers for improving energy conversion efficiency of electronics. Nano Energy *108*, 108177. https://doi.org/10.1016/j.nanoen.2023.108177.
24. Li, R., Shi, Y., Wu, M., Hong, S., Wang, P., Xiong, L., and Gao, F.B. (2020). Photovoltaic panel cooling by atmospheric water sorption–evaporation cycle. Nat. Sustain. *3*, 636–643. https://doi.org/10.1038/s41893-020-0535-4.
25. Wang, G., Li, Y., Qiu, H., Yan, H., and Zhou, Y. (2022). High-performance and wide relative humidity passive evaporative cooling utilizing atmospheric water. Droplet *2*, e32. https://doi.org/10.1002/dro2.32.
26. Xu, N., Zhu, P., Sheng, Y., Zhou, L., Li, X., Tan, H., Zhu, S., and Zhu, J. (2020). Synergistic Tandem Solar Electricity-Water Generators. Joule *4*, 347–358. https://doi.org/10.1016/j.joule.2019.12.010.
27. Ni, F., Xiao, P., Zhang, C., Zhou, W., Liu, D., Kuo, S.W., and Chen, T. (2021). Atmospheric Hygroscopic Ionogels with Dynamically Stable Cooling Interfaces Enable a Durable Thermoelectric Performance Enhancement. Adv. Mater. *33*, e2103937. https://doi.org/10.1002/adma.202103937.
28. Liu, X., Li, P., Chen, J., Jiang, P., Mai, Y.W., and Huang, X. (2022). Hierarchically porous composite fabrics with ultrahigh metal-organic framework loading for zero-energy-consumption heat dissipation. Sci. Bull. *67*, 1991–2000. https://doi.org/10.1016/j.scib.2022.09.014.
29. Günay, A.A., Harish, S., Fuchi, M., Kinefuchi, I., Lee, Y., and Shiomi, J. (2022). Metal–organic framework coated porous structures for enhanced thermoelectric performance. Energy Convers. Manag. *255*, 115289. https://doi.org/10.1016/j.enconman.2022.115289.
30. Pu, S., Su, J., Li, L., Wang, H., Chen, C., and Hu, X. (2019). Bioinspired sweating with temperature sensitive hydrogel to passively dissipate heat from high-end wearable electronics. Energy Convers. Manag. *180*, 747–756. https://doi.org/10.1016/j.enconman.2018.11.027.
31. Cheng, P., Tang, Z., Chen, X., Xu, J., Liu, P., Zhang, X., and Wang, G. (2023). Advanced phase change hydrogel integrating metal-organic framework for self-powered thermal management. Nano Energy *105*, 108009. https://doi.org/10.1016/j.nanoen.2022.108009.
32. Wang, J., Wang, J., Sheng, Z., Du, R., Yan, L., and Zhang, X. (2021). Solid-Liquid-Vapor Triphase Gel. Langmuir *37*, 13501–13511. https://doi.org/10.1021/acs.langmuir.1c02333.
33. Zeng, J., Zhang, X., Chung, K.M., Feng, T., Zhang, H., Prasher, R.S., and Chen, R. (2023). Moisture thermal battery with autonomous water harvesting for passive electronics cooling. Cell Reports Physical Science *4*, 101250. https://doi.org/10.1016/j.xcrp.2023.101250.
34. Wang, C., Liu, P., Chen, X., Liu, J., Lu, Q., Shao, S., Yang, Z., Chen, H., and King-Jones, K. (2020). A Thermal Management Strategy for Electronic Devices Based on Moisture Sorption-Desorption Processes. Joule *10*, 435–447. https://doi.org/10.1016/j.joule.2019.12.005.
35. Tao, Y., Qian, Y., Li, Y., Hao, J., Xu, T., Li, W., Jiang, Q., Luo, Y., and Yang, J. (2022). High-performance and long-term thermal management material of MIL-101Cr@GO. Materials Today Physics *22*, 100572. https://doi.org/10.1016/j.mtphys.2021.100572.
36. Sheng, L., Wang, Y., Wang, X., Han, C., and Chen, Z. (2023). A thermal management strategy for electronic devices based on copper double skin inspired hydrogel. Int. J. Heat Mass Tran. *206*, 123946. https://doi.org/10.1016/j.ijheatmasstransfer.2023.123946.
37. Xu, J., Chao, J., Li, T., Yan, T., Wu, S., Wu, M., Zhao, B., and Wang, R. (2020). Near-Zero-Energy Smart Battery Thermal Management Enabled by Sorption Energy Harvesting from Air. ACS Cent. Sci. *6*, 1542–1554. https://doi.org/10.1021/acscentsci.0c00570.
38. Pu, S., Liao, Y., Chen, K., Fu, J., Zhang, S., Ge, L., Conta, G., Bouzarif, S., Cheng, T., Hu, X., et al. (2020). Thermogalvanic Hydrogel for Synchronous Evaporative Cooling and Low-Grade Heat Energy Harvesting. Nano Lett. *20*, 3791–3797. https://doi.org/10.1021/acs.nanolett.0c00800.
39. Yang, P., Feng, C., Liu, Y., Cheng, T., Yang, X., Liu, H., Liu, K., and Fan, H.J. (2020). Thermal Self-Protection of Zinc-Ion Batteries Enabled by Smart Hygroscopic Hydrogel Electrolytes. Adv. Energy Mater. *10*, 2002898. https://doi.org/10.1002/aenm.202002898.
40. Yu, W., Zhang, G., Liu, C., and Fan, S. (2020). Hard Carbon Nanotube Sponges for Highly Efficient Cooling via Moisture Absorption-Desorption Process. ACS Nano *14*, 14091–14099. https://doi.org/10.1021/acsnano.0c06748.
41. Zhang, L., Yu, W., Wang, J., Gao, D., Chen, Y., Dai, W., Wang, P., Li, G., Meng, C., Liu, C., and Guo, S. (2023). Carbon Nanotube/Hygroscopic Salt Nanocomposites with Dual-Functionality of Effective Cooling and Fire Resistance for Safe and Ultrahigh-Rate Operation of Practical Lithium-Ion Batteries. Adv. Funct. Mater. *33*, 2213846. https://doi.org/10.1002/adfm.202213846.
42. Li, W., Jaromír Klemeš, J., Wang, Q., and Zeng, M. (2022). Efficient thermal management strategy of Li-ion battery pack based on sorption heat storage. Energy Convers. Manag. *256*, 115383. https://doi.org/10.1016/j.enconman.2022.115383.
43. Yue, Q.L., He, C.X., Sun, J., Xu, J.B., and Zhao, T.S. (2022). A passive thermal management system with thermally enhanced water adsorbents for lithium-ion batteries powering electric vehicles. Appl. Therm. Eng. *207*, 118156. https://doi.org/10.1016/j.applthermaleng.2022.118156.
44. Song, Y., Xu, N., Liu, G., Qi, H., Zhao, W., Zhu, B., Zhou, L., and Zhu, J. (2022). High-yield solar-driven atmospheric water harvesting of metal–organic-framework-derived nanoporous carbon with fast-diffusion water channels. Nat. Nanotechnol. *17*, 857–863. https://doi.org/10.1038/s41565-022-01135-y.
45. Ni, F., Xiao, P., Zhang, C., and Chen, T. (2022). Hygroscopic polymer gels toward atmospheric moisture exploitations for energy management and freshwater generation. Matter *5*, 2624–2658. https://doi.org/10.1016/j.matt.2022.06.010.
46. Díaz-Marín, C.D., Zhang, L., Lu, Z., Alshrah, M., Grossman, J.C., and Wang, E.N. (2022). Kinetics of Sorption in Hygroscopic Hydrogels. Nano Lett. *22*, 1100–1107. https://doi.org/10.1021/acs.nanolett.1c04216.
47. Min, X., Wu, Z., Wei, T., Hu, X., Shi, P., Xu, N., Wang, H., Li, J., Zhu, B., and Zhu, J. (2023). High-Yield Atmospheric Water Harvesting Device with

Integrated Heating/Cooling Enabled by Thermally Tailored Hydrogel Sorbent. ACS Energy Lett. *8*, 3147–3153. https://doi.org/10.1021/acsenergylett.3c00682.

48. Poredoš, P., Shan, H., and Wang, R. (2022). Dehumidification with solid hygroscopic sorbents for low-carbon air conditioning. Joule *6*, 1390–1393. https://doi.org/10.1016/j.joule.2022.06.020.
49. Xu, J., Li, T., Yan, T., Wu, S., Wu, M., Chao, J., Huo, X., Wang, P., and Wang, R. (2021). Ultrahigh solar-driven atmospheric water production enabled by scalable rapid-cycling water harvester with vertically aligned nanocomposite sorbent. Energy Environ. Sci. *14*, 5979–5994. https://doi.org/10.1039/d1ee01723c.
50. Shan, H., Li, C., Chen, Z., Ying, W., Poredoš, P., Ye, Z., Pan, Q., Wang, J., and Wang, R. (2022). Exceptional water production yield enabled by batch-processed portable water harvester in semi-arid climate. Nat. Commun. *13*, 5406. https://doi.org/10.1038/s41467-022-33062-w.
51. Song, Y., Zeng, M., Wang, X., Shi, P., Fei, M., and Zhu, J. (2023). Hierarchical Engineering of Sorption-Based Atmospheric Water Harvesters. Adv. Mater.2209134 https://doi.org/10.1002/adma.202209134.
52. Zhang, Y., Dong, H., Wang, R., and Feng, P. (2020). Air humidity assisted sorption thermal battery governed by reaction wave model. Energy Storage Mater. *27*, 9–16. https://doi.org/10.1016/j.ensm.2020.01.012.
53. Entezari, A., Lin, H., Esan, O.C., Luo, W., Wang, R., You, R., and An, L. (2023). Continuous humidity pump and atmospheric water harvesting inspired by a tree-pumping system. Cell Reports Physical Science *4*, 101278. https://doi.org/10.1016/j.xcrp.2023.101278.
54. Xu, F., Li, Y., Wang, H., Zhang, P., and Jin, D. (2017). Understanding Mobile Traffic Patterns of Large Scale Cellular Towers in Urban Environment. IEEE/ACM Trans. Netw. *25*, 1147–1161. https://doi.org/10.1109/tnet.2016.2623950.
55. Woods, J., Mahvi, A., Goyal, A., Kozubal, E., Odukomaiya, A., and Jackson, R. (2021). Rate capability and Ragone plots for phase change thermal energy storage. Nat. Energy *6*, 295–302. https://doi.org/10.1038/s41560-021-00778-w.
56. Zeng, Z., Zhao, B., and Wang, R. (2023). Water based adsorption thermal battery: Sorption mechanisms and applications. Energy Storage Mater. *54*, 794–821. https://doi.org/10.1016/j.ensm.2022.11.024.
57. Zhang, Y., and Wang, R. (2020). Sorption thermal energy storage: Concept, process, applications and perspectives. Energy Storage Mater. *27*, 352–369. https://doi.org/10.1016/j.ensm.2020.02.024.
58. Aftab, W., Usman, A., Shi, J., Yuan, K., Qin, M., and Zou, R. (2021). Phase change material-integrated latent heat storage systems for sustainable energy solutions. Energy Environ. Sci. *14*, 4268–4291. https://doi.org/10.1039/d1ee00527h.
59. Zhang, Y.N., Wang, R.Z., and Li, T.X. (2018). Thermochemical characterizations of high-stable activated alumina/LiCl composites with multistage sorption process for thermal storage. Energy *156*, 240–249. https://doi.org/10.1016/j.energy.2018.05.047.
60. Shan, H., Pan, Q., Xiang, C., Poredoš, P., Ma, Q., Ye, Z., Hou, G., and Wang, R. (2021). High-yield solar-driven atmospheric water harvesting with ultra-high salt content composites encapsulated in porous membrane. Cell Reports Physical Science *2*, 100664. https://doi.org/10.1016/j.xcrp.2021.100664.
61. Liu, H.R., Hua, L.J., Li, B.J., Wang, C.X., and Wang, R.Z. (2021). Thermal resistance-capacitance network model for fast simulation on the desiccant coated devices used for effective electronic cooling. Int. J. Refrig. *131*, 78–86. https://doi.org/10.1016/j.ijrefrig.2021.07.038.
62. Wang, W., Pan, Q., Wang, R., and Ge, T. (2022). Modeling and optimization of a honeycombed adsorbent bed for efficient moisture capture. Appl. Therm. Eng. *200*, 117717. https://doi.org/10.1016/j.applthermaleng.2021.117717.
63. Li, R., Wang, W., Shi, Y., Wang, C.T., and Wang, P. (2023). Advanced Material Design and Engineering for Water-Based Evaporative Cooling. Adv. Mater.e2209460 https://doi.org/10.1002/adma.202209460.